Principles and Dynamics of Natural Arm Capacitor Voltage Balancing of a Direct Modulated Modular Multilevel Converter

Shenghui Cui[1], Jae-Jung Jung[2], Younggi Lee[2], and Seung-Ki Sul[2]
[1] E.ON Energy Research Center, RWTH Aachen University, Germany
[2] Department of Electrical and Computer Engineering, Seoul National University, Korea

***Abstract*-- Natural capacitor voltage balancing of six arms of a direct modulated Modular Multilevel Converter (MMC) has been observed by several articles both by experiments and simulations. However, its principles have not been revealed clearly and its dynamics have not been analyzed analytically. In this paper it's shown that a DC component and a line frequency circulating current would be induced inside the converter inherently in case of arm capacitor voltage unbalance and the induced circulating current would transfer energy among six arms to balance arm capacitor voltage naturally without any closed-loop control. And the dynamics of natural arm capacitor voltage balancing have been analyzed mathematically and verified by both computer simulations and experiments.**

***Index Terms*—modular multilevel converter, HVDC, natural balancing, direct modulation, indirect modulation.**

I. INTRODUCTION

Voltage Source Converter (VSC) based High Voltage Direct Current (HVDC) transmission is a promising solution for future smart grid which would integrate a great amount of renewable energy sources to the existing grids. For VSC-HVDC, compared to the conventional two level or three level converters, a Modular Multilevel Converter (MMC) is a competitive candidate and is attracting worldwide attention [1-3]. MMC presents many advantages such as very low harmonics, low dv/dt, modularity and simple scaling, no necessity of series connection of power semiconductors, and DC bus capacitor elimination [4-6], etc.

Control strategies of the MMC are generally classified into indirect modulation based control and direct modulation based control [7,8]. The direct modulation based control is one of the popular techniques due to its simple structure of controllers. In the direct modulation technique, the insertion ratio is acquired by the fixed rated DC bus voltage and the total numbers of inserted cells in the upper and lower arms are kept as constant. The major drawback of the direct modulation technique is the presence of considerable twice line frequency component circulating current due to the fluctuation of the cell capacitor voltage. Typically the circulating current is suppressed by increasing inductance of the arm inductor or by employing a circulating current suppression controller [9]. While in the indirect modulation technique, the insertion ratio is acquired by the measured cell capacitor voltage in real time. For the indirect modulation based control, the twice line frequency component circulating current is inherently prevented whereas regulation of the arm capacitor voltage

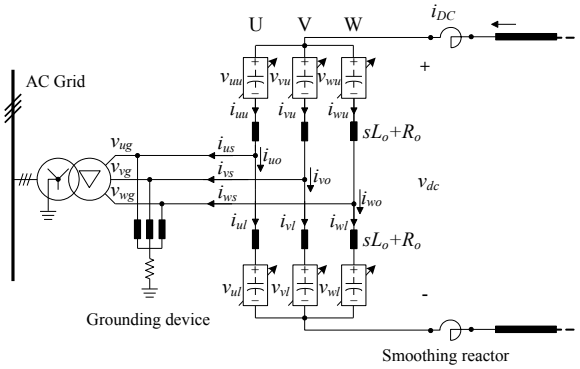

Figure 1. Simplified schematic of an MMC station in HVDC application.

is marginally stable and an additional closed-loop controller should be employed to stabilize capacitor voltages of six arms of the MMC [8,16].

One interesting characteristic of the direct modulated MMC is the natural balancing of the arm capacitor voltage without any closed-loop control. However, as far as authors know, its principles and dynamics have not been investigated clearly until a first approach on this issue had been published in [10].

In [10], a stiff DC voltage source was presumed to be connected to the DC bus of the MMC and principles and dynamics of natural arm capacitor voltage regulation were analyzed independently for each phase. However, different from the conventional two-level or three-level converter based VSC-HVDC system, there's no capacitor connected in the DC bus of the MMC. Moreover, a smoothing reactor is usually installed in series in the DC bus. And, the DC bus reveals more current sourced nature instead of stiff voltage source nature. However, for a point-to-point HVDC transmission system natural balancing of capacitor voltages of six arms has been observed and reported by several articles [11-13]. It means that the direct modulated MMC might have natural arm capacitor voltage balancing capability even with not stiff voltage source in DC bus.

In this paper, principles and dynamics of natural arm capacitor voltage balancing of the direct modulated MMC are investigated and analyzed under the assumption of the generalized DC bus. It has been proven analytically that for a direct modulated MMC, a DC component and a line frequency component of the circulating current would be induced inherently when the arm capacitor voltages are unbalanced and the currents make the arm capacitor voltages of six arms be balanced.

This paper is organized as follows. In Section II,

dynamics of arm capacitor voltage and circulating current are introduced. In Section III, the principles of arm capacitor voltage natural regulation of the MMC connected with stiff DC bus voltage source are reviewed. In Section IV, the principles and dynamics of the natural arm capacitor voltage balancing with generalized DC bus are presented. In Section V, the full scale simulation is performed to verify the validity of this work. In Section VI, experimental results with a down scaled experiment prototype are presented to support the conclusion in this paper.

II. Dynamics of Current and Arm Capacitor Voltage

A simplified schematic of an MMC station in HVDC application is shown in Fig. 1. An MMC consists of three legs for three phases, and each leg contains two arms, respectively the upper arm and the lower arm. Each arm usually contains numerous (up to several hundreds) half bridge cells. Typically while the number of cells per arm is N, then the rated cell capacitor voltage is set as (1).

$$V_{cell}^{*} = \frac{V_{dc,rated}}{N}. \tag{1}$$

A. Voltage synthesis

In the direct modulation technique, the references of upper and lower arm output voltages of phase 'x' are obtained by two complementary sinusoidal references as (2) in which the v_{xs}^{*} is the reference of the output AC voltage to drive the AC grid side current. Then the insertion ratios of the upper and lower arms are calculated as (3).

$$\begin{cases} v_{xu}^{*} = \frac{V_{dc,rated}}{2} - v_{xs}^{*} \\ v_{xl}^{*} = \frac{V_{dc,rated}}{2} + v_{xs}^{*} \end{cases}. \tag{2}$$

$$\begin{cases} n_{xu}^{*} = \frac{\frac{V_{dc,rated}}{2} - v_{xs}^{*}}{V_{dc,rated}} \\ n_{xl}^{*} = \frac{\frac{V_{dc,rated}}{2} + v_{xs}^{*}}{V_{dc,rated}} \end{cases}. \tag{3}$$

Then in accordance with (3), the instantaneous numbers of the inserted cells in upper and lower arms can be calculated as (4). For the direct modulation, the sum of numbers of inserted cells in each phase is always N as (5).

$$\begin{cases} N_{xu} = \frac{N}{2} - round\left(\frac{v_{xs}^{*}}{V_{dc,rated}}\right) \\ N_{xl} = \frac{N}{2} + round\left(\frac{v_{xs}^{*}}{V_{dc,rated}}\right) \end{cases}. \tag{4}$$

$$N_{xu} + N_{xl} = N. \tag{5}$$

To simplify analysis, some assumptions are presumed with reasonable approximations as follows [14].

- The individual capacitor voltages within each arm of the converter are balanced well by proper sorting and selection technique.
- Both the number of cells per arm and the sampling frequency of the digital controller are high enough to represent the inserted arm voltage as continuous variables.

Then, the instantaneously synthesized arm voltage can be calculated as (6) in accordance with (3). In (6) $v_{c,xu}^{\Sigma}$ and $v_{c,xl}^{\Sigma}$ represent the sum of cell capacitor voltages in the upper arm and the lower arm respectively.

$$\begin{cases} v_{xu} = n_{xu}^{*} v_{c,xu}^{\Sigma} = \left(\frac{1}{2} - \frac{v_{xs}^{*}}{V_{dc,rated}}\right) \times v_{c,xu}^{\Sigma} \\ v_{xl} = n_{xu}^{*} v_{c,xl}^{\Sigma} = \left(\frac{1}{2} + \frac{v_{xs}^{*}}{V_{dc,rated}}\right) \times v_{c,xl}^{\Sigma} \end{cases}. \tag{6}$$

In [15], it has been analyzed mathematically that a line frequency and a twice line frequency fluctuation exist in arm capacitor voltages of both the upper and lower arms. The twice line frequency fluctuations in the upper and lower arms are with the same magnitude and phase, while the line frequency fluctuations are with the same magnitude and opposite phase at each arm. Then the arm capacitor voltages of both upper and lower arms can be represented as (7), in which $\bar{a}$ represents the average value and $\tilde{a}$ represents the fluctuating component.

$$\begin{cases} v_{c,xu}^{\Sigma} = \bar{v}_{c,xu}^{\Sigma} + \tilde{v}_{c,x,\omega}^{\Sigma} + \tilde{v}_{c,x,2\omega}^{\Sigma} \\ v_{c,xl}^{\Sigma} = \bar{v}_{c,xl}^{\Sigma} - \tilde{v}_{c,x,\omega}^{\Sigma} + \tilde{v}_{c,x,2\omega}^{\Sigma} \end{cases}. \tag{7}$$

B. Dynamics of arm capacitor voltage

If the conversion losses are neglected, then time derivatives of the upper and lower arm capacitor energy are the power calculated by multiplication of the instantaneous arm output voltage and the current that flows through the corresponding arm as (8). According to the nature of the capacitors, (8) can be represented as (9) in detail.

$$\frac{dE_{xu,xl}}{dt} = v_{xu,xl} i_{xu,xl}. \tag{8}$$

$$\begin{cases} \frac{dE_{xu}}{dt} = C\sum_{i=1}^{N} v_{c,xu[i]} \frac{dv_{c,xu[i]}}{dt} \cong \frac{C}{2N} \frac{d\left(v_{c,xu}^{\Sigma}\right)^2}{dt} \\ \frac{dE_{xl}}{dt} = C\sum_{i=1}^{N} v_{c,xl[i]} \frac{dv_{c,xl[i]}}{dt} \cong \frac{C}{2N} \frac{d\left(v_{c,xl}^{\Sigma}\right)^2}{dt} \end{cases}. \tag{9}$$

Then by substituting (9) and (6) into (8), dynamics of arm capacitor voltage are obtained as (10).

$$\begin{cases} \frac{C}{N} \frac{d(v_{c,xu}^{\Sigma})}{dt} = n_{xu}^{*} i_{xu} \\ \frac{C}{N} \frac{d(v_{c,xl}^{\Sigma})}{dt} = n_{xl}^{*} i_{xl} \end{cases}. \tag{10}$$

The leg current of 'x' phase is defined by the mean value of the upper and lower arm currents in this paper and is denoted as (11). Hence according to (10), the dynamics of sum and difference of upper and lower arm capacitor voltages can be deduced as (12).

$$i_{xo} = \frac{i_{xu} + i_{xl}}{2}. \tag{11}$$

$$\begin{cases} \frac{C}{N} \frac{d(v_{c,x}^{\Sigma})}{dt} = \frac{C}{N} \frac{d(v_{c,xu}^{\Sigma} + v_{c,xl}^{\Sigma})}{dt} = i_{xo} - \frac{v_{xs}^{*} i_{xs}}{V_{dc,rated}} \\ \frac{C}{N} \frac{d(v_{c,x}^{\Delta})}{dt} = \frac{C}{N} \frac{d(v_{c,xu}^{\Sigma} - v_{c,xl}^{\Sigma})}{dt} = \frac{i_{xs}}{2} - \frac{2 v_{xs}^{*} i_{xo}}{V_{dc,rated}} \end{cases}. \tag{12}$$

In (12), the sum of upper and lower arm capacitor voltages is affected by both the corresponding phase active power and the leg current. Moreover, the difference of upper and lower arm capacitor voltages would drift while a line frequency component is included in the leg current. It can be concluded from (12) that the leg current plays a crucial role in dynamics of arm capacitor voltages.

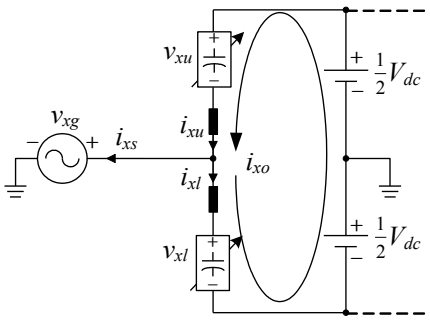

Figure 2. Per phase equivalent circuit of MMC with stiff voltage source DC bus.

III. Principles of Natural Arm Capacitor Voltage Regulation of MMC with Stiff Voltage Source DC Bus

In [10], principles and dynamics of natural arm capacitor voltage regulation of the MMC with stiff voltage source DC bus were reported. For an MMC with the DC bus connected to a stiff voltage source, internal dynamics of current can be analyzed independently for each phase. The per phase equivalent circuit of the MMC with a stiff voltage source DC bus is shown in Fig. 2. While the arm capacitor voltages of both the upper and lower arms are regulated as rated voltage, (13) should be satisfied which is also equivalent to (14).

$$\begin{cases} \bar{v}_{c,xu}^{\Sigma} = V_{dc,rated} \\ \bar{v}_{c,xl}^{\Sigma} = V_{dc,rated} \end{cases}. \tag{13}$$

$$\begin{cases} \bar{v}_{c,x}^{\Sigma} = \bar{v}_{c,xu}^{\Sigma} + \bar{v}_{c,xl}^{\Sigma} = 2V_{dc,rated} \\ \bar{v}_{c,x}^{\Delta} = \bar{v}_{c,xu}^{\Sigma} - \bar{v}_{c,xl}^{\Sigma} = 0 \end{cases}. \tag{14}$$

According to Kirchhoff's law, dynamics of the leg current are deduced as (15), in which $\Delta\bar{v}_{c,x}^{\Sigma}$ and $\Delta\bar{v}_{c,x}^{\Delta}$ represent the deviations of $\bar{v}_{c,x}^{\Sigma}$ and $\bar{v}_{c,x}^{\Delta}$ from their equilibrium points in (14).

$$\left(L_o\frac{d}{dt}+R_o\right)i_{xo} = \frac{1}{2}\begin{Bmatrix} -\frac{\Delta\bar{v}_{c,x}^{\Sigma}}{2}+\frac{v_{xs}^*}{V_{dc,rated}}\Delta\bar{v}_{c,x}^{\Delta} \\ -\tilde{v}_{c,x,2\omega}^{\Sigma}+2\frac{v_{xs}^*\tilde{v}_{c,x,\omega}^{\Sigma}}{V_{dc,rated}} \end{Bmatrix}. \tag{15}$$

In (15), in the steady the twice line frequency leg current would be induced inside the leg due to fluctuation of arm capacitor voltage. The induced twice line frequency current leads to the reactive power that flows inside the converter and increases losses. However, its contribution to the drift of arm capacitor voltage is negligible [10]. Moreover, a DC component leg current would be induced in case $\bar{v}_{c,x}^{\Sigma}$ drifts from its equilibrium point and a line frequency leg current would be induced in case $\bar{v}_{c,x}^{\Delta}$ drifts from its equilibrium point *0*. Then from (15), dynamics of deviation of leg current around the equilibrium point can be derived as (16).

$$\left(L_o\frac{d}{dt}+R_o\right)\Delta i_{xo} = \frac{1}{2}\left(-\frac{\Delta\bar{v}_{c,x}^{\Sigma}}{2}+\frac{v_{xs}^*}{V_{dc,rated}}\Delta\bar{v}_{c,x}^{\Delta}\right). \tag{16}$$

By small signal analysis via linearization, dynamics of deviations of $\bar{v}_{c,x}^{\Sigma}$ and $\bar{v}_{c,x}^{\Delta}$ around their equilibrium points can be deduced from (12) as (17) and (18).

$$\frac{C}{N}\frac{d(\Delta v_{c,x}^{\Sigma})}{dt} = \Delta i_{xo}. \tag{17}$$

$$\frac{C}{N}\frac{d(\Delta v_{c,x}^{\Delta})}{dt} = -\frac{2v_{xs}^*\Delta i_{xo}}{V_{dc}}. \tag{18}$$

Hence substituting (16) into (17), dynamics of deviation variable $\Delta v_{c,x}^{\Sigma}$ can be deduced as (19). If the transient time of arm capacitor voltage is assumed to be much larger than a period of line frequency oscillation and time constant of arm inductor, then dynamics of deviation variable $\Delta v_{c,x}^{\Delta}$ can be deduced as (20) in which the magnitude of v_{xs}^* is denoted as V_{ms}.

$$\left(\frac{d^2}{dt^2}+\frac{R_o}{L_o}\frac{d}{dt}+\frac{N}{4CL_o}\right)\Delta v_{c,x}^{\Sigma} = 0. \tag{19}$$

$$\left(\frac{d}{dt}+\frac{N}{2C}\frac{V_{ms}^2}{V_{dc,rated}^2}\frac{1}{\sqrt{R_o^2+(\omega L_o)^2}}\frac{R_o}{\sqrt{R_o^2+(\omega L_o)^2}}\right)\Delta v_{c,x}^{\Delta} = 0. \tag{20}$$

Since the roots of (19) are located in left half part of the Laplace plane, the deviation of $\bar{v}_{c,x}^{\Sigma}$ decays to null in accordance with a second order transient process. According to (20), the deviation of $\bar{v}_{c,x}^{\Delta}$ decays to null with a first order transient process. Eq. (19) and (20) reveal that for a direct modulated MMC with a stiff voltage source DC bus, the upper and lower arm capacitor voltages converge to their rated value $V_{dc,rated}$ inherently without any additional closed loop control.

IV. Principles of Natural Arm Capacitor Voltage Balancing of MMC with Generalized DC Bus

A. Dynamics of current

A universal MMC model is proposed in [16] for generalized nature of DC bus. In the universal MMC model, an MMC circuit is divided into three equivalent circuits, respectively, the AC grid current circuit, the DC bus current circuit, and the circulating current circuit as shown in Fig. 3.

For a direct modulated MMC, the effective output AC voltage which drives the AC grid current can be calculated as (21). Besides the reference of the output AC voltage v_{xs}^*, a DC component (in case of unbalance of upper and lower arm capacitor voltages) and harmonic components exist as disturbance terms. However, since the disturbance terms are much smaller compared to the reference of output AC voltage v_{xs}^* and the bandwidth of the grid current regulator is usually up to hundreds of Hz (much faster than that of arm capacitor voltage control), it can be assumed that the AC grid current tracks its sinusoidal reference ideally as (22).

$$v_{xs} = \frac{v_{xl}-v_{xu}}{2} = \frac{(\bar{v}_{c,xu}^{\Sigma}+\bar{v}_{c,xl}^{\Sigma})}{2V_{dc,rated}}v_{xs}^* + \frac{\tilde{v}_{c,x,2\omega}^{\Sigma}}{V_{dc,rated}}v_{xs}^* + \frac{(\bar{v}_{c,xl}^{\Sigma}-\bar{v}_{c,xu}^{\Sigma})}{4} - \frac{\tilde{v}_{c,x,\omega}^{\Sigma}}{2}. \tag{21}$$

$$i_{xs} = i_{xs}^*. \tag{22}$$

The instantaneous voltage of the DC bus is derived as (23) in accordance with Kirchhoff's current law. Then substituting (6) and (7) into (23), the instantaneous voltage of DC bus can be derived as (24).

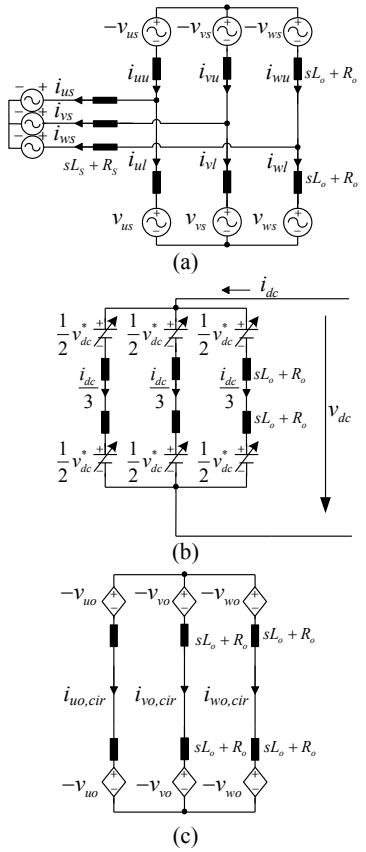

Figure 3. Universal MMC model under generalized nature of DC bus: (a) Equivalent circuit for AC grid current, (b) Equivalent circuit for DC bus current, (c) Equivalent circuit for circulating current.

$$v_{dc} = \frac{\sum_{x=u,v,w}\left(v_{xu}+v_{xl}+2\left(L_o\frac{d}{dt}+R_o\right)i_{xo}\right)}{3}. \tag{23}$$

$$v_{dc} = \frac{\sum_{x=u,v,w}\left(\frac{\bar{v}^{\Sigma}_{c,xu}+\bar{v}^{\Sigma}_{c,xl}}{2}-\frac{v^{*}_{xs}\bar{v}^{\Delta}_{c,x}}{V_{dc,rated}}+\tilde{v}^{\Sigma}_{c,x,2\omega}-2\frac{v^{*}_{xs}\tilde{v}^{\Sigma}_{c,x,\omega}}{V_{dc,rated}}+2\left(L_o\frac{d}{dt}+R_o\right)i_{xo}\right)}{3} \tag{24}$$

$$v_{dc} = \frac{\sum_{x=u,v,w}\left(\frac{\bar{v}^{\Sigma}_{c,xu}+\bar{v}^{\Sigma}_{c,xl}}{2}-\frac{v^{*}_{xs}\bar{v}^{\Delta}_{c,x}}{V_{dc,rated}}\right)}{3}+\frac{2\left(L_o\frac{d}{dt}+R_o\right)}{3}i_{dc}. \tag{25}$$

Since there's no zero sequence component included in the oscillation harmonic terms generated by three phases in (24) [15], the instantaneous DC bus voltage can be simplified as (25). Hence in accordance with (25), the oscillation harmonic terms would not appear in the DC bus and the DC bus current should be a pure DC component in steady state.

A circulating current of 'x' phase is defined as the difference between the corresponding phase leg current and the mean value of the DC bus current that equally flows into each leg as (26). The circulating current only flows inside the MMC and is determined by the leg internal voltage as shown by (27). For a direct modulated MMC, the leg internal voltage can be calculated as (28) [16]. Substituting (6), (7) and (28) into (27), dynamics of circulating current can be derived as (29).

$$i_{xo,cir} = i_{xo} - \frac{i_{dc}}{3}. \tag{26}$$

$$\left(L_o\frac{d}{dt}+R_o\right)i_{xo,cir} = v_{xo}. \tag{27}$$

$$v_{xo} = -\frac{1}{2}\left\{v_{xu}+v_{xl}-\frac{\sum_{x=u,v,w}\left(v_{xu}+v_{xl}\right)}{3}\right\}. \tag{28}$$

$$\left(L_o\frac{d}{dt}+R_o\right)i_{xo,cir} = -\frac{1}{2}\left\{\left(\frac{\bar{v}^{\Sigma}_{c}}{2}-\frac{1}{2}\frac{\sum_{x=u,v,w}\bar{v}^{\Sigma}_{c}}{3}\right)-\left(\frac{v^{*}_{xs}\bar{v}^{\Delta}_{c,x}}{V_{dc,rated}}-\frac{1}{3}\left(\sum_{x=u,v,w}\frac{v^{*}_{xs}\bar{v}^{\Delta}_{c,x}}{V_{dc,rated}}\right)\right)+\tilde{v}^{\Sigma}_{c,x,2\omega}-2\frac{v^{*}_{xs}\tilde{v}^{\Sigma}_{c,x,\omega}}{V_{dc,rated}}\right\}. \tag{29}$$

As shown by (29), there're four terms included in the leg internal voltage. The first two terms in right side of (29) indicate that a DC component or a line frequency component of the leg internal voltage would be generated in case of arm capacitor voltage unbalance to drive a circulating current inside the MMC. The last two terms in right side of (21) indicate that a negative sequence twice line frequency circulating current would flows inside the MMC in the steady state.

B. Principles of leg capacitor voltage balancing

Arm capacitor voltage balancing of the MMC includes two parts, respectively the leg capacitor voltage balancing and the upper and lower arm capacitor balancing at each leg. At first, the principle of leg capacitor voltage balancing is investigated. Substituting (26) into (12), dynamics of leg capacitor voltages of three phases are derived as (30).

$$\begin{cases}\frac{C}{N}\frac{d\left(v^{\Sigma}_{c,u}\right)}{dt} = \frac{i_{dc}}{3}-\frac{v^{*}_{us}i_{us}}{V_{dc,rated}}+i_{uo,cir}\\ \frac{C}{N}\frac{d\left(v^{\Sigma}_{c,v}\right)}{dt} = \frac{i_{dc}}{3}-\frac{v^{*}_{vs}i_{vs}}{V_{dc,rated}}+i_{vo,cir}\\ \frac{C}{N}\frac{d\left(v^{\Sigma}_{c,w}\right)}{dt} = \frac{i_{dc}}{3}-\frac{v^{*}_{ws}i_{ws}}{V_{dc,rated}}+i_{wo,cir}\end{cases}. \tag{30}$$

In three phase balanced condition, the first two terms in right side of (30) are canceled with each other in accordance with power balance between the AC side and the DC side [15]. For the study of leg capacitor voltage balancing of a direct modulated MMC, the differential component of the leg capacitor voltage is defined as the difference between corresponding phase leg capacitor voltage and the mean value of three phase leg capacitor voltages and is denoted as $v^{\Sigma}_{c,x,diff}$. Then dynamics of average value of $v^{\Sigma}_{c,x,diff}$ are deduced from (30) as (31) excluding the oscillation harmonic components.

$$\begin{cases}\frac{C}{N}\frac{d\left(\bar{v}^{\Sigma}_{c,u,diff}\right)}{dt} = i_{uo,cirDC}\\ \frac{C}{N}\frac{d\left(\bar{v}^{\Sigma}_{c,v,diff}\right)}{dt} = i_{vo,cirDC}\\ \frac{C}{N}\frac{d\left(\bar{v}^{\Sigma}_{c,w,diff}\right)}{dt} = i_{wo,cirDC}\end{cases}. \tag{31}$$

As shown by (29), the differential component of the leg capacitor voltage would induce a DC circulating current inside the MMC. In addition, it's indicated by (31) that a DC circulating current would drive the differential component of the leg capacitor voltage as a feedback. Then by substituting (29) into (31), dynamics of differential component of the leg capacitor voltage are derived as (32), whose poles are located in left half part of Laplace plane as (33).

$$\left(\frac{d^2}{dt^2}+\frac{R_o}{L_o}\frac{d}{dt}+\frac{N}{4CL_o}\right)\begin{bmatrix}\bar{v}^{\Sigma}_{c,u,diff}\\ \bar{v}^{\Sigma}_{c,v,diff}\\ \bar{v}^{\Sigma}_{c,w,diff}\end{bmatrix}=\begin{bmatrix}0\\0\\0\end{bmatrix}. \tag{32}$$

$$\begin{cases} p^{\Sigma}_{1,2}=\frac{1}{2}\left(-\frac{R_o}{L_o}\pm j\sqrt{\frac{N}{CL_o}-\frac{R_o^2}{L_o^2}}\right)\\ \tau^{\Sigma}=\frac{2L_o}{R_o}\\ \omega^{\Sigma}_{osc}=\frac{1}{2}\sqrt{\frac{N}{CL_o}-\frac{R_o^2}{L_o^2}}\end{cases}. \tag{33}$$

As shown by (32), for a direct modulated MMC, the three phase leg capacitor voltages converge to a balanced state inherently without any additional closed-loop control. The transient of convergence process is supposed to be a second order under-damped case and the decay time constant is determined by parameters of the arm inductor as indicated by (33).

C. Principles of upper and lower arm capacitor voltage balancing

Besides the leg capacitor voltage natural balancing, principles and dynamics of natural balancing of upper and lower arm capacitor voltages should also be investigated. Substituting (26) into (12), dynamics of differences of upper and lower arm capacitor voltages of three phases are derived as (34). Since the first two terms of right side of (34) do not generate an average DC component, only the line frequency component included in the circulating current of the third term of right side of (34) would drift the average value of $v^{\Delta}_{c,x}$.

$$\begin{cases} \frac{C}{N}\frac{d(v^{\Delta}_{c,u})}{dt}=\frac{i_{us}}{2}-\frac{2v^{*}_{us}i_{dc}}{3V_{dc,rated}}-\frac{2v^{*}_{us}i_{uo,cir}}{V_{dc,rated}}\\ \frac{C}{N}\frac{d(v^{\Delta}_{c,v})}{dt}=\frac{i_{vs}}{2}-\frac{2v^{*}_{vs}i_{dc}}{3V_{dc,rated}}-\frac{2v^{*}_{vs}i_{vo,cir}}{V_{dc,rated}}\\ \frac{C}{N}\frac{d(v^{\Delta}_{c,w})}{dt}=\frac{i_{ws}}{2}-\frac{2v^{*}_{ws}i_{dc}}{3V_{dc,rated}}-\frac{2v^{*}_{ws}i_{wo,cir}}{V_{dc,rated}}\end{cases}. \tag{34}$$

For the study of upper and lower arm capacitor voltage balancing of a direct modulated MMC, the common component of $v^{\Delta}_{c,x}$ of 'x' phase is defined as the three phase mean value of $v^{\Delta}_{c,x}$ and is denoted as $v^{\Delta}_{c,com}$. And the differential component of $v^{\Delta}_{c,x}$ is defined as the difference between corresponding phase $v^{\Delta}_{c,x}$ and the $v^{\Delta}_{c,com}$, and is denoted as $v^{\Delta}_{c,x,diff}$. As shown in (29), the average value of difference of upper and lower arm capacitor voltages, namely $\bar{v}^{\Delta}_{c,x}$ would generate a line frequency leg internal voltage to induce a line frequency component circulating current inside the MMC. At first, the line frequency circulating current contributed by common component of $v^{\Delta}_{c,x}$, namely $v^{\Delta}_{c,com}$ is analyzed. Without loss of generality, phasors of references of output AC voltage can be represented as (35).

$$\boldsymbol{V^{*}_{us}}=V_{ms},\boldsymbol{V^{*}_{vs}}=V_{ms}e^{-j\frac{2\pi}{3}},\boldsymbol{V^{*}_{ws}}=V_{ms}e^{j\frac{2\pi}{3}}. \tag{35}$$

Then the phasors of the positive sequence and negative sequence leg internal voltages generated by $v^{\Delta}_{c,com}$ are calculated as (36) and (37) by (29).

$$\boldsymbol{V^{+}_{uo,AC}}=\frac{\boldsymbol{V_{uo,AC}}+\boldsymbol{V_{vo,AC}}e^{j\frac{2\pi}{3}}+\boldsymbol{V_{wo,AC}}e^{-j\frac{2\pi}{3}}}{3}= V_{ms}\frac{\bar{v}^{\Delta}_{c,com}}{V_{dc,rated}}. \tag{36}$$

$$\boldsymbol{V^{-}_{uo,AC}}=\frac{\boldsymbol{V_{uo,AC}}+\boldsymbol{V_{vo,AC}}e^{-j\frac{2\pi}{3}}+\boldsymbol{V_{wo,AC}}e^{+j\frac{2\pi}{3}}}{3}=0. \tag{37}$$

An interesting property could be observed from (36) and (37). The common component of three phase upper and lower arm capacitor voltage differences, namely $v^{\Delta}_{c,com}$ generates only a positive sequence leg internal voltage to induce a positive sequence circulating current inside the MMC. Furthermore, a positive sequence circulating current only drifts the common component of three phase upper and lower arm capacitor voltage differences [16]. Then by substituting (36) and (29) into (34) and assuming that transient time of arm capacitor voltage is much larger than a period of line frequency oscillation and time constant of arm inductor, dynamics of the average common component of differences of three phase upper and lower arm capacitor voltages are deduced as (38), in which the pole is calculated as (39).

$$\frac{d\bar{v}^{\Delta}_{c,com}}{dt}+p^{\Delta}_{com}\bar{v}^{\Delta}_{c,com}=0. \tag{38}$$

$$p^{\Delta}_{com}=-\frac{N}{C}\frac{V^2_{ms}}{2V^2_{dc,rated}}\frac{1}{\sqrt{R_o^2+(\omega L_o)^2}}\frac{R_o}{\sqrt{R_o^2+(\omega L_o)^2}}. \tag{39}$$

Since the pole of (38) locates in the left half part of the Laplace plane, the common components of differences of three phase upper and lower arm capacitor voltages decay to zero inherently in accordance with a first-order transient process.

The differential component of $\bar{v}^{\Delta}_{c,x}$ should also be considered. The phasors of the positive sequence and negative sequence leg internal voltages generated by the differential component are calculated as (40) and (41) from (29), in which the differential component is represented in stationary d-q reference frame.

$$\boldsymbol{V^{+}_{uo,AC}}=\frac{\boldsymbol{V_{uo,AC}}+\boldsymbol{V_{vo,AC}}e^{j\frac{2\pi}{3}}+\boldsymbol{V_{wo,AC}}e^{-j\frac{2\pi}{3}}}{3}=0. \tag{40}$$

$$\boldsymbol{V^{-}_{uo,AC}}=\frac{\boldsymbol{V_{uo,AC}}+\boldsymbol{V_{vo,AC}}e^{-j\frac{2\pi}{3}}+\boldsymbol{V_{wo,AC}}e^{+j\frac{2\pi}{3}}}{3}=\frac{V_{ms}}{2}\frac{\bar{v}^{\Delta}_{c,d}+j\bar{v}^{\Delta}_{c,q}}{V_{dc,rated}}. \tag{41}$$

The differential component of three phase upper and lower arm capacitor voltage differences generate only a negative sequence leg internal voltage to induce a negative sequence circulating current inside the MMC. Furthermore, a negative sequence circulating current only drifts the differential component of three phase upper and lower arm capacitor voltage differences [16]. Then by substituting (41) and (29) into (34) and assuming that transient time of arm capacitor voltage is much larger than a period of line frequency oscillation and time constant of arm inductor, dynamics of the average differential component of differences of three phase upper and lower arm capacitor voltages (in stationary d-q reference frame) are deduced as (42), whose poles are calculated as (43).

$$\begin{bmatrix} \frac{d\bar{v}_{c,d}^{\Delta}}{dt} \\ \frac{d\bar{v}_{c,q}^{\Delta}}{dt} \end{bmatrix} = K \begin{bmatrix} \frac{-R_o}{\sqrt{R_o^2+(\omega L_o)^2}} & \frac{-\omega L_o}{\sqrt{R_o^2+(\omega L_o)^2}} \\ \frac{\omega L_o}{\sqrt{R_o^2+(\omega L_o)^2}} & \frac{-R_o}{\sqrt{R_o^2+(\omega L_o)^2}} \end{bmatrix} \begin{bmatrix} \bar{v}_{c,d}^{\Delta} \\ \bar{v}_{c,q}^{\Delta} \end{bmatrix}, \quad (42)$$

$$where\ K = \frac{N}{C} \frac{V_{ms}^2}{4V_{dc,rated}^2} \frac{1}{\sqrt{R_o^2+(\omega L_o)^2}}.$$

$$\begin{cases} p_{diff,1,2}^{\Delta} = -K \frac{R_o}{\sqrt{R_o^2+(\omega L_o)^2}} \pm jK \frac{\omega L_o}{\sqrt{R_o^2+(\omega L_o)^2}} \\ \tau_{diff}^{\Delta} = \left(K \frac{R_o}{\sqrt{R_o^2+(\omega L_o)^2}} \right)^{-1} \\ \omega_{diff,osc}^{\Delta} = K \frac{\omega L_o}{\sqrt{R_o^2+(\omega L_o)^2}} \end{cases}. \quad (43)$$

Since the pole of (42) locates in the left half part of Laplace plane, the differential component of differences of three phase upper and lower arm capacitor voltages decays to zero inherently in accordance with a under-damped second-order transient process.

D. Observations

In summary, for a direct modulated MMC, the arm capacitor voltages of six different arms are balanced inherently without employing any closed-loop control. For three phase leg capacitor voltages, a DC component of circulating current is induced inherently in case of unbalance of the leg capacitor voltages to balance the voltages. For upper and lower arm capacitor voltage balancing, a line frequency AC component of circulating current is induced naturally in case of unbalance of upper and lower arm capacitor voltages at each phase to balance the voltages.

The convergence rate of the natural arm capacitor voltage balancing is one of the main concerns. For the leg capacitor voltage balancing, the convergence process is an under-damped second-order transient process, and the convergence rate is only determined by parameters of the arm inductor as indicated by (33). For the upper and lower arm capacitor voltage balancing, the convergence process includes a first order transient process (common difference) and an under-damped second order transient process (differential difference), and the convergence rate is proportional to the parasitic resistance of the arm inductor and is inversely proportional to the capacitance of cell capacitor.

V. Simulation Results

To verify the validity of the principles and dynamics analyzed in this work, a full scale computer simulation is performed. The equivalent simulation model proposed by [17] is employed to reduce the simulation time without sacrificing simulation accuracy. Parameters of the simulated MMC are shown in Table I.

At the beginning of the simulation, initial capacitor voltages in each arm are set as different values around the rated voltage, and the balancing dynamics are observed in no load condition to verify the analysis conducted in this paper. The MMC operates in rectifier mode and the DC bus of the MMC is not connected to anything.

Fig. 3 shows the differential component of three phase leg capacitor voltages, namely the differences among three leg capacitor voltages in stationary d-q reference frame. The angular frequency of the oscillation is around 88.8 rad/s and it coincides well with 85.2 rad/s which is calculated by (33). The theoretically calculated convergence envelops by (33) are shown by dashed lines

TABLE II. Simulation Parameters

Quantity	Values
Number of cells per arm	200
Rated DC bus voltage	400 kV
Rated cell capacitor voltage	2.0 kV
Cell capacitor	45 mF
AC grid voltage	180.5 kV
Arm inductor inductance	150 mH
Arm inductor resistance	3.67 Ω
Controller sampling frequency	10.0 kHz

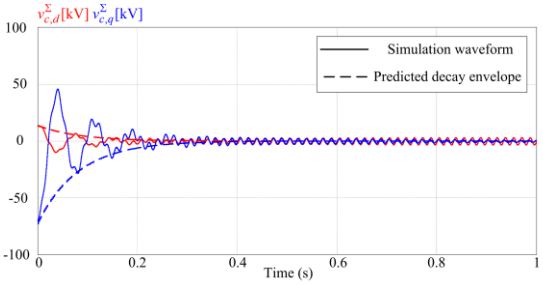

Figure 3. Differences among three phase leg capacitor voltages in stationary d-q reference frame.

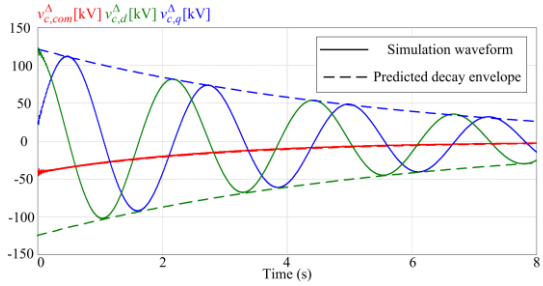

Figure 4. Differences of upper and lower arm capacitor voltages of three phases in stationary d-q reference frame.

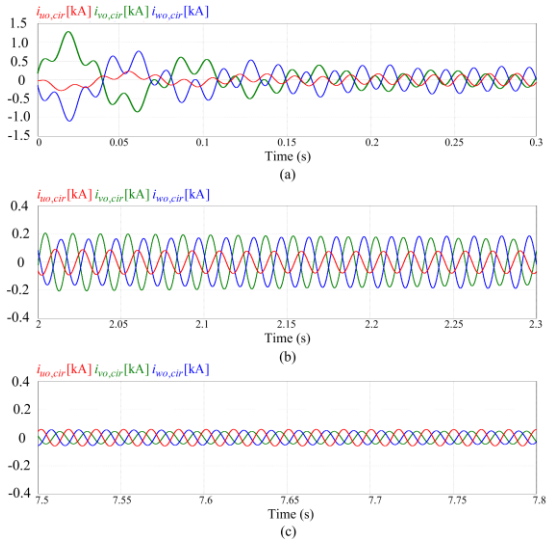

Figure 5. Simulation waveforms of circulating current.

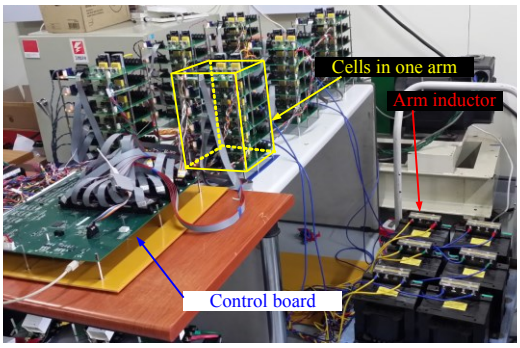

(a)

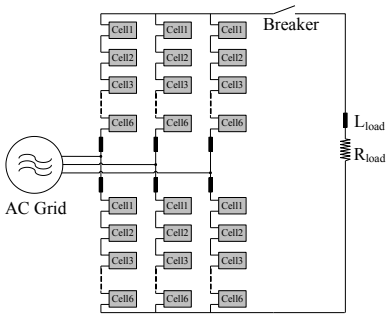

(b)

Figure 6. Constructed experimental prototype of the modular multilevel converter: (a) Photograph of the prototype, (b) Schematic of the prototype.

TABLE III. PARAMETERS OF PROTOTYPE MMC SYSTEM UNDER TEST

Quantity	Values
Number of cells per arm	6
Rated DC bus voltage	300V
Rated cell capacitor voltage	50V
Cell capacitor capacitance	5.4mF
Grid voltage	110V
Arm inductor inductance	4.0 mH
DC bus R-L load inductance	20.0 mH
DC bus R-L load resistance	30 Ω
Digital controller sampling frequency	10.0 kHz

in Fig. 3, and they coincide well with the simulation results.

Fig. 4 shows the differences of upper and lower arm capacitor voltages in stationary d-q reference frame. At first, it is demonstrated clearly that the convergence process of the common component of upper and lower arm capacitor voltage differences is a first-order process without oscillation, while that of the differential component is an under-damped second order process with oscillations. The theoretically calculated convergence envelopes by (39) and (43) are presented by dashed lines in Fig. 4, and they coincide well with the simulation results. The angular frequency of the oscillation is around 2.79 rad/s and it coincides reasonably with 2.66 rad/s, which is calculated by (43).

Simulation waveforms of circulating current are shown in Fig. 5. In Fig. 5(a), during t=0~0.3s, since three phase leg capacitor voltages are not balanced and the upper and lower arm capacitor voltages are neither balanced, both a DC component and a line frequency AC component exist in the circulating current. In Fig. 5(b), during t=2~2.3s, since the three phase leg capacitor voltages have been already balanced, there is only a line frequency AC component in the circulating current. Since during this period, both the common and differential components of upper and lower arm capacitor voltage differences exist as shown in Fig. 4, the line frequency circulating current includes both the positive sequence and negative sequence components. As indicated by (39) and (43), convergence rate of the common component of upper and lower arm capacitor voltage differences is twice that of the differential component. In Fig. 5(c), during t=7.5~7.8s since the common component of upper and lower arm capacitor voltage differences almost decayed to zero, the circulating current is dominated by the negative sequence component as analyzed in Section IV.

VI. EXPERIMENTAL RESULTS

As a laboratory test setup, a seven level MMC prototype has been constructed and it is tested by direct modulation to verify the analysis conducted in this paper. Photograph of the constructed experimental prototype is shown in Fig. 6(a) and parameters of the prototype are listed in Table II. The DC bus of the MMC is connected to an R-L load directly through a circuit breaker as shown in Fig. 6(b). The effective parasitic resistance of the arm inductor R_o is around 0.3 Ohm considering the converter losses. To observe the transient process at different conditions and to make case illustrative, the experiments are performed as follows: Before the MMC operates under direct modulation control, a closed-loop indirect modulation control strategy [16] is employed to regulate the arm capacitor voltages of six arms to different values in the steady state. Then operation of the MMC changes to the direct modulation mode to confirm the analysis in this study.

A. Experimental results at no load condition

To verify the analysis of this work, the balancing dynamics are observed at no load condition at first and the DC bus of the MMC is separated from the R-L load by the circuit breaker.

In Fig. 7. (a), the case is that before the operation of the MMC changes to the direct modulation mode, the arm capacitor voltages are set as follows: $\bar{v}_{c,uu}^{\Sigma} = 330V$, $\bar{v}_{c,ul}^{\Sigma} = 330V$, $\bar{v}_{c,vu}^{\Sigma} = 300V$, $\bar{v}_{c,vl}^{\Sigma} = 300V$, $\bar{v}_{c,wu}^{\Sigma} = 270V$, $\bar{v}_{c,uu}^{\Sigma} = 270V$. Then at the beginning of the transient process, inter-leg capacitor voltage difference exists but upper and lower arm capacitor voltages are balanced at each phase. Then in this case, only the DC circulating current flows inside the MMC during the transient process. It's demonstrated clearly in the stationary d-q reference frame that the induced DC circulating current drives the differences among three leg capacitor voltages to be null. The calculated convergence

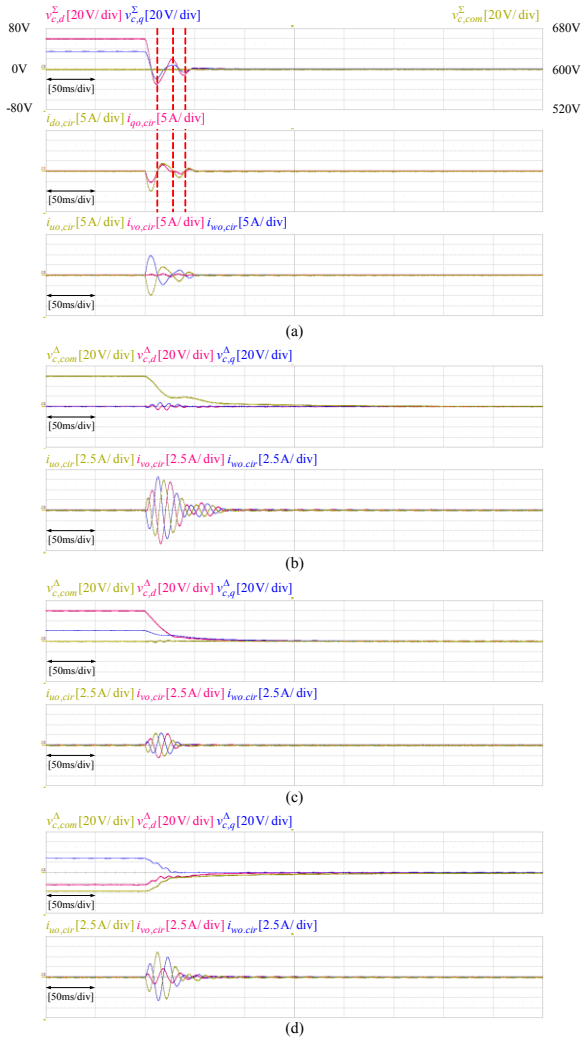

Figure 7. Experimental results of arm capacitor voltage and circulating current at no load condition: (a) Balancing of leg capacitor voltages, (b) Balancing of upper and lower arm capacitor voltages (common component), (c) Balancing of upper and lower arm capacitor voltages (differential component), (d) Balancing of upper and lower arm capacitor voltages (both common and differential components).

time constant is 27ms and the angular frequency of the oscillation is 261rad/s, which coincide with the experiment results well.

In Fig. 7. (b), the case is that before the operation of the MMC changes to the direct modulation mode, the arm capacitor voltages are set as follows: $\bar{v}_{c,uu}^{\Sigma} = 330V$, $\bar{v}_{c,ul}^{\Sigma} = 270V$, $\bar{v}_{c,vu}^{\Sigma} = 330V$, $\bar{v}_{c,vl}^{\Sigma} = 270V$, $\bar{v}_{c,wu}^{\Sigma} = 330V$, $\bar{v}_{c,uu}^{\Sigma} = 270V$. Then at the beginning of the transient process, only common component of upper and lower arm capacitor voltages exist and the three phase leg capacitor voltages are balanced. Then, in this case only the positive sequence line frequency component circulating current flows inside the MMC during the transient process.

In Fig. 7(c), the case is that before the operation of the MMC changes to the direct modulation mode, the arm capacitor voltages are set as follows: $\bar{v}_{c,uu}^{\Sigma} = 330V$, $\bar{v}_{c,ul}^{\Sigma} = 270V$, $\bar{v}_{c,vu}^{\Sigma} = 294V$, $\bar{v}_{c,vl}^{\Sigma} = 306V$, $\bar{v}_{c,wu}^{\Sigma} = 276V$, $\bar{v}_{c,uu}^{\Sigma} = 324V$. Then at the beginning of the

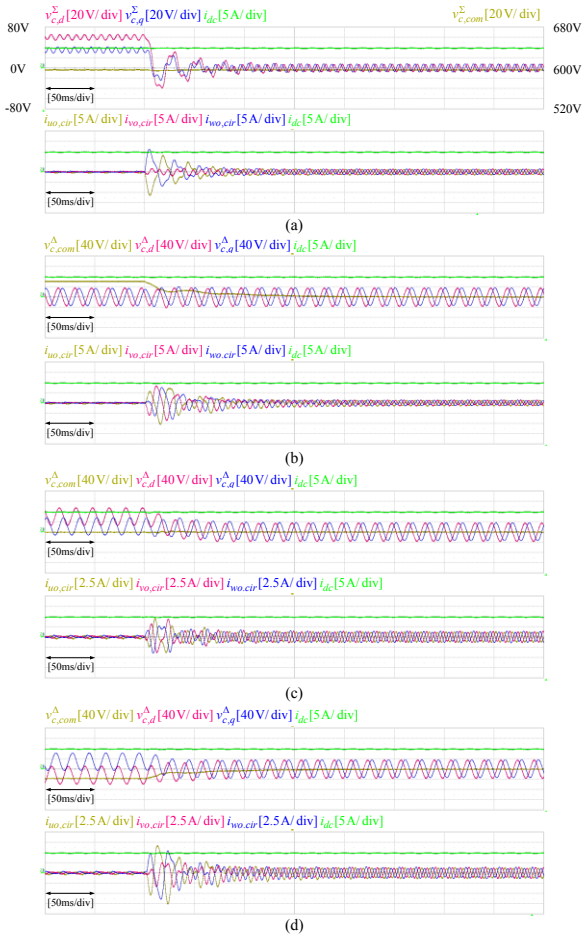

Figure 8. Experimental results of arm capacitor voltage and circulating current at loaded condition: (a) Balancing of leg capacitor voltages, (b) Balancing of upper and lower arm capacitor voltages (common component), (c) Balancing of upper and lower arm capacitor voltages (differential component), (d) Balancing of upper and lower arm capacitor voltages (both common and differential components).

transient process, only differential component of upper and lower arm capacitor voltages exist and the three phase leg capacitor voltages are balanced. Then in this case, only the negative sequence line frequency circulating current flows inside the MMC during the transient process.

In Fig. 7(d), the case is that before the operation of the MMC changes to the direct modulation mode, the arm capacitor voltages are set as follows: $\bar{v}_{c,uu}^{\Sigma} = 270V$, $\bar{v}_{c,ul}^{\Sigma} = 330V$, $\bar{v}_{c,vu}^{\Sigma} = 300V$, $\bar{v}_{c,vl}^{\Sigma} = 300V$, $\bar{v}_{c,wu}^{\Sigma} = 276V$, $\bar{v}_{c,uu}^{\Sigma} = 324V$. Then at the beginning of the transient process, only the difference of upper and lower arm capacitor voltages exists and the three phase leg capacitor voltages are balanced. Then, in this case only the line frequency circulating current (both positive and negative sequence components) flows inside the MMC during the transient process.

The calculated decay time constants of both common and differential components of upper and lower arm capacitor voltage differences from (39) and (43) are respectively 158ms and 316ms, which are larger than that of experiment results. Moreover, the decay process of the differential component of upper and lower arm capacitor

voltage differences does not present an under-damped oscillation. The main reason for the error is inferred as that the duration of balancing process is not sufficiently larger than the period of line frequency oscillation (16.7ms) and the time constant of the arm inductor (26.7ms) as assumed in Section IV.

B. Experiment results at loaded condition

The balancing dynamics are also observed at loaded condition. The circuit breaker is switched on and R-L load is connected to the DC bus. And the experiments in sub-section A are repeated.

The experiment results at loaded condition are shown in Fig. 8. Comparing the experimental results at both no load and loaded conditions in Fig. 7 and Fig. 8, it can be concluded that the dynamics are almost similar besides that the twice line frequency circulating current are induced after the MMC changes operation mode from the indirect modulation mode to the direct modulation mode at loaded condition. It means that the induced DC component and the line frequency AC component of circulating current in case of arm capacitor voltage unbalance play crucial roles in arm capacitor voltage natural balancing, and effect of the oscillating harmonic components of the circulating current is negligible as analyzed in Section IV.

VII. CONCLUSIONS

In this paper, principles and dynamics of natural arm capacitor voltage balancing of the direct modulated MMC with generalized DC bus have been explained. The unbalance of three phase leg capacitor voltages induces a DC component circulating current inherently to balance the leg capacitor voltages naturally. A line frequency AC component circulating current would be induced in case of the unbalance of upper and lower arm capacitor voltages of three phases. Capacitor energies are transferred among six different arms by the induced circulating current and the upper and lower arm capacitor voltages are balanced inherently. Dynamics of these two processes are derived mathematically and it has been proven that arm capacitor voltage balancing among six arms is asymptotically stable. The dynamics obtained from the both simulation and experiment results verify the validity of the analysis conducted in this paper.

REFERENCES

[1] T. K. Vrana and O. Fosso, “Technical aspects of the North Sea super grid,” *CIGRE ELECTRA*, no. 258, pp. 6-19, Oct. 2011.

[2] S. Allebrod, R. Hamerski, and R. Marquardt, “New transformerless, scalable modular multilevel converters for HVDC-transmission,” in *Proc. IEEE Power Electronics Specialisits Conference*, pp. 174-179, 2008.

[3] B. Gemmell, J. Dorn, D. Retzmann, and D. Soerangr, “Prospects of multilevel VSC technologies for power transmission,” in *Conf. Rec. IEEE Transmission and Distribution Conference and Exposition*, pp. 1-16, 2008.

[4] A. Lesnicar and R. Marquardt, “An innovative modular multilevel converter topology suitable for a wide power range,” in *Proc. IEEE Boogna Power Tech*, vol. 3, pp. 1-6, 2008.

[5] D. Peftitsis, G. Tolstoy, A. Antonopoulos, J. Rabkowski, J. K. Lim, M. Bakowski, L. Angquist, and H. P. Nee, “High-power modular multilevel converters with SiC JFETs,” in *Proc. IEEE Energy Conversion Congress and Exposition*, pp. 2148-2155, 2010.

[6] Rainer Marquardt, “Modular Multilevel Converter Topologies with DC-Short Circuit Current Llimitation,” in *Proc. IEEE International Conference on Power Electronics ECCE Asia*, pp. 1425-1431, 2011.

[7] S. Debnath, J. Qin, B. Bahrani, M. Saeedifard, P. Barbosa, “Operation, control, and applications of the modular multilevel converter: A review,” in *IEEE Trans. on Power Electronics*, vol. 30, pp. 37-53, 2015.

[8] A. Antonopoulos, L. Anguist, and H.P. Nee, "On dynamics and voltage control of the modular multilevel converter," in *EPE European Conference on Power Electronics and Applications*, pp. 1-10, 2009.

[9] Q. Tu, Z. Xu, Lie Xu, “Reduced switching-frequency modulation and circulating current suppression for modular multilevel converters,” in *IEEE Trans. on Power Delivery*, vol. 26, pp. 2009-2017, 2011.

[10] L. Hamefors, A. Antonopoulos, S. Norrga, L. Angquist, H.P. Nee, “Dynamic analysis of modular multilevel converters,” *IEEE Trans. on Industrial Electronics*, vol. 60, pp. 2526-2536, 2013.

[11] Q. Tu, Z. Xu, “Impact of sampling frequency on harmonic distortion for modular multilevel converter,” *IEEE Trans. on Power Delivery*, pp. 298-306, 2011.

[12] Liu Sheng, *et al*, “Electromechanical transient modeling of modular multilevel converter based multi-terminal HVDC systems,” *IEEE Trans. on Power Systems*, pp. 72-83, 2014.

[13] S. Maryam, and R. Iravani, “Dynamic performance of a modular multilevel back-to-back HVDC system,” *IEEE Trans. on Power Delivery*, pp.2903-2912, 2010.

[14] L. Angquist, A. Antonopoulos, D. Siemaszko, K. Ilves, M. Vasiladiotis, and H. Nee, “Open-loop control of modular multilevel converters using estimation of stored energy,” *IEEE Trans. on Industray Applications*, pp. 2516-2524, 2011.

[15] Q. Song, W. Liu, X. Li, H. Rao, L. Li, “A steady-state analysis method for a modular multilevel converter,” *IEEE. Trans. on Power Electronics*, pp.3702-3713, 2013.

[16] Shenghui Cui, Sungmin Kim, Jae-Jung Jung, Seung-Ki Sul, “A comprehensive cell capacitor energy control strategy of a modular multilevel converter (MMC) without a stiff DC bus voltage source,” in *IEEE Applied Power Electronics Conference and Expo*., 2014, pp.602-609.

[17] U. Gnanarathna *et al*, “Efficient modeling of modular multilevel HVDC converters (MMC) on electromagnetic transient simulation programs,” *IEEE Trans. On Power Delivery*, vol. 26, pp.316-324, 2011.